Elucidating *in Vivo* Structural Dynamics in Integral Membrane Protein by Hydroxyl Radical Footprinting*

Yi Zhu‡, Tiannan Guo‡, Jung Eun Park‡, Xin Li‡, Wei Meng‡, Arnab Datta‡, Marshall Bern§, Sai Kiang Lim¶, and Siu Kwan Sze‡‖

We describe here a novel footprinting technique to probe the *in vivo* structural dynamics of membrane protein. This method utilized *in situ* generation of hydroxyl radicals to oxidize and covalently modify biomolecules on living *Escherichia coli* cell surface. After enriching and purifying the membrane proteome, the modified amino acid residues of the protein were identified with tandem mass spectrometry to map the solvent-accessible surface of the protein that will form the footprint of *in vivo* structure of the protein. Of about 100 outer membrane proteins identified, we investigated the structure details of a typical β-barrel structure, the porin OmpF. We found that six modified tryptic peptides of OmpF were reproducibly detected with 19 amino acids modified under the physiological condition. The modified amino acid residues were widely distributed in the external loop area, β-strands, and periplasmic turning area, and all of them were validated as solvent-accessible according to the crystallography data. We further extended this method to study the dynamics of the voltage gating of OmpF *in vivo* using mimic changes of physiological circumstance either by pH or by ionic strength. Our data showed the voltage gating of porin OmpF *in vivo* for the first time and supported the proposed mechanism that the local electrostatic field changes in the eyelet region may alter the porin channels to switch. Thus, this novel method can be a potentially efficient method to study the structural dynamics of the membrane proteins of a living cell. ***Molecular & Cellular Proteomics 8:1999–2010, 2009.***

One of the most challenging problems in biological sciences is the correlation of the dynamic three-dimensional (3D)[1] structural changes in membrane proteins to their biological functions. Comprising about 30% of the human proteome, membrane proteins are critical mediators of material and information transfer between cells and their environment and are targets for many growth factors and pharmacologically active compounds. Signals from binding of ligands or drugs to receptors are transduced through conformational changes in the receptors. Therefore, understanding the dynamic conformational changes in the structure of membrane proteins is essential to the understanding of many biological processes and has important implications in human health.

Although some methodologies including NMR and x-ray have been developed to study protein structures in atomic resolution, the determination of the structures of integral membrane proteins (IMPs) remains one of the most challenging problems in biological sciences (1). IMPs are usually insoluble low abundance proteins for which expression, purification, and crystallization are generally too inefficient to generate sufficient materials for conventional structural analysis techniques such as NMR and x-ray. Additionally, IMPs in living cells are constantly interacting with different molecules depending on the external environment and biological states of the cell such that the conformation of IMPs is highly dynamic. Hence monitoring real time conformational changes in these proteins by NMR and x-ray methods is unfeasible, and alternative methods are needed.

Recent progress in MS has enabled a novel MS-based protein oxidative footprinting technique to determine structural information by mapping of oxidation induced by hydroxyl (OH) radicals. This method is an adaptation of the OH radical footprinting first developed by Tullius and co-workers (2, 3) for the folding study of DNA/RNA molecules in solution. Several groups have since extended this method in combination with mass spectrometry for the mapping of a protein surface (4–8). In these studies, OH radicals oxidize amino acid residues located on the protein surface and produce stable covalent modifications to side chains without causing backbone cleavages. Due to the very small size and nonspecific activity of hydroxyl radicals, this is a random process dependent only on the solvent-accessible surface and the chemical properties of the exposed amino acids. It has been reported that there are about 12 possible types of side-chain oxidation products in

From the ‡School of Biological Sciences, Nanyang Technological University, 60 Nanyang Drive, Singapore 637551, Singapore, §Palo Alto Research Center, Palo Alto, California 94304, and ¶Institute of Medical Biology, 8A Biomedical Grove, 05-505 Immunos, Singapore 138648, Singapore

Received, February 12, 2009, and in revised form, May 22, 2009

Published, MCP Papers in Press, May 26, 2009, DOI 10.1074/mcp.M900081-MCP200

[1] The abbreviations used are: 3D, three-dimensional; OMP, outer membrane protein; IMP, integral membrane protein; LTQ, linear quadrupole ion trap; XIC, extracted ion chromatogram; 1D, one-dimensional; FA, formic acid; Vc, critical voltage; Mowse, molecular weight search.

© 2009 by The American Society for Biochemistry and Molecular Biology, Inc.
This paper is available on line at http://www.mcponline.org

protein footprinting experiments (9); however, not all of these oxidation products are common events as reviewed. The most common event results in formation of an alcohol group for almost all the amino acid residues with mass increases of +16 Da. Another common event is the formation of an aldehyde/ketone group for eight residues, Val, Ile, Leu, Lys, Arg, Pro, Glu, and Gln, with mass increases of +14 Da (9). Others include +32 Da on Cys, Met, Trp, Phe, and Tyr; +48 Da on Cys and Trp; +5, −10, −22, and −23 Da on His; −30 Da on Asp and Glu; −16 Da on Cys; −32 Da on Met; and −2 Da on Ser and Thr (9).

The oxidized protein is subsequently sequenced by MS/MS to locate the oxidized amino acid residues. The oxidized amino acid residues provide the surface information of the protein, and thus the surface topology can be mapped. At the same time, the oxidation level of each side chain can be accurately measured by quantitative liquid chromatography-coupled MS. Because the level of oxidation for each tryptic peptide depends primarily on the solvent accessibility of the peptide side chains that is in turn dependent on the conformation of the protein, the oxidation level and changes in its level for each peptide can therefore be used to determine conformation and conformational changes of the protein. This approach has been shown to be a powerful technique in understanding ligand-induced conformational changes when coupled with existing structural data that are either experimentally or computationally generated (10).

Despite recent advances, most current surface mapping techniques still require purified proteins and are therefore not amenable to the conformation determination of most IMPs or their complexes. In particular, the current techniques still cannot determine real time *in vivo* structural changes of IMPs that are important in understanding the functions of IMPs. Therefore, the structural dynamics of IMP remain elusive.

IMPs display two membrane-spanning tertiary structural motifs, *i.e.* α-helix bundles in the cytoplasmic membrane and β-barrels in the outer membrane (11). In Gram-negative bacteria, the outer membrane forms a protective permeability barrier around the cells and serves as a molecular filter for hydrophilic substances (12). To facilitate this, channel-forming proteins are embedded in the outer membrane to mediate the transport of nutrients and ions across the membrane into the periplasm. The most abundant proteins in this class are the porins that form aqueous passive channels with a physical diameter of about 1 nm for the transport of ions and relatively small polar molecules across the outer membrane of bacteria (13–15). Porins form β-barrels with 16 or 18 membrane-spanning antiparallel β-strands that are connected by short turns on the periplasmic side named T1, T2, etc. and long loops on the extracellular side named L1, L2, etc. (16, 17). In all porins, the constriction at the barrel center is formed by an inserted loop L3 (13, 16, 18), which is not exposed to the cell surface but folds back into the channel and contributes significantly to the permeability of the pore. Functional porins are homotrimers of these β-barrel subunits with each subunit producing a channel in the outer membrane, and the trimer therefore contains three channels (14). Currently known porins fall into two distinct groups: 16-stranded general diffusion porins such as the matrix porin OmpF that transports ions and small molecules (<600 Da) without much selectivity and 18-stranded specific porins such as maltoporin that have a precise selectivity for a defined substrate (15, 17, 19–22). General porin trimers exhibit symmetrical or asymmetrical voltage gating when reconstituted into planar lipid bilayers in electrophysiological studies (23–27). By measuring the ion conductance *in vitro*, porin trimers were found to be able to exhibit at least two functional states, an open and a closed state, in response to changes in the transmembrane potential difference, known as "voltage gating", and the voltage above which the porin channel will be closed is called the critical voltage, Vc. Although existing data generally support voltage gating *in vitro*, there are no data to support voltage gating *in vivo* (25, 27).

We describe here a novel adaptation of an oxidative footprinting and MS technique to study *in vivo* conformational changes of IMPs in living cells. We used *Escherichia coli* as a model to study the structural dynamics of the outer membrane proteins with an emphasis on the matrix porin OmpF. Considering that the yellowish and cloudy *E. coli* bacteria culture would interfere with the laser photolysis of H_2O_2 because H_2O_2 only absorbs laser light at a wavelength around 250 nm and this cloudy medium would inhibit the laser penetration (4), we adopted a Fenton reaction but not the pulsed laser photolysis method to oxidize the living bacteria. Fenton oxidation is not guaranteed for many proteins, especially the highly dynamic proteins, because this method needs a relatively longer incubation time (2, 4, 5, 9). This time scale is too long because most of the conformational changes of macromolecules take place only in the time scale of milliseconds to seconds (10). However, Fenton chemistry is suitable to study the outer membrane porins because they have extremely stable structures that are restricted by both the intramolecular hydrogen bond and the hydrophobic interaction with the lipid bilayer wall, and a large conformational change of this kind of protein is considered unlikely (14, 20).

In this method, living *E. coli* cells were first exposed to OH radicals generated from an *in situ* Fenton reaction between hydrogen peroxide and Fe(II)-bound EDTA. The outer membrane proteins that have a large solvent-accessible surface area would be preferentially oxidized by the OH radicals. The outer membrane proteins were then isolated and enriched from the cell lysate. The porin OmpF was subsequently purified by 1D SDS-PAGE electrophoresis followed by proteolysis to generate peptides for analysis and identification by LC-MS/MS and bioinformatics analysis. The structural information of porin OmpF as interpreted from our oxidative footprinting and MS study was in agreement with the x-ray crystallography structure (20). Highly reproducible oxidized amino acid residues were widely distributed in the external

loops, transmembrane β-strands, and periplasmic turnings of the protein, and all of them were validated as solvent-accessible according to the x-ray structure of porin OmpF.

We then extended this method to probe for voltage gating of porin OmpF under different conditioned circumstances to assess the robustness of its application in complicated biological systems. Here *E. coli* was stimulated first with either a low ionic strength solution or a low pH buffer after harvest and exposed to OH radicals generated by Fenton reagents in solution for 3 min. Our data showed that the extent of oxidation of two polypeptides from extracellular loops remained constant independent of conditions that induced either channel closing or opening. However, we observed that oxidation level of peptides in β-stranded areas deep inside the porin channel was reduced when the environment changed from one that induced channel opening to another that induced channel closing. These data not only supported the voltage gating of porin OmpF *in vivo* but also revealed the molecular basis underlying voltage gating of porin OmpF.

EXPERIMENTAL PROCEDURES

Materials—HPLC grade solvents were purchased from J. T. Baker Inc. Complete protease inhibitor mixture tablets were from Roche Diagnostics. All remaining laboratory chemicals were purchased from Sigma-Aldrich unless stated otherwise.

Cell Culture—*E. coli* K-12 strain WT31 from ATCC were grown aerobically in 450 ml of LB broth medium at 37 °C with shaking at 225 rpm in 2-liter baffled flasks (Nalgene) from a 1:100 dilution of overnight culture until midlog phase (A_{600} = 0.9–1.1). Cells were collected by centrifugation at 3000 × *g* at 4 °C for 10 min and washed three times in fresh minimum salts medium M9 (pH 7.4). The total amount of cells from one flask culture was aliquoted into three fractions, and each fraction was resuspended into 15 ml of fresh M9 medium (pH 7.4) for subsequent experiments.

Oxidation of Living E. coli Bacteria under the Physiological Condition—For the oxidation study, *E. coli* cells were divided into two groups, the control group and oxidation group, with each group containing three fractions of the suspension of cells as mentioned above. The oxidation procedure was performed as described previously (28, 29) with some modifications. Briefly, in the oxidation group, the cells were incubated with a freshly prepared Fenton solution of Fe-EDTA (final concentration, 10 mM $Fe(NH_4)_2(SO_4)_2$ and 25 mM Na_2EDTA) in M9 medium (pH 7.4) at 37 °C for 10min. A certain amount of 3% H_2O_2 was then added into the cell suspension to a final concentration of 0.3% and incubated for 3 min to allow the oxidation reaction that was initiated by OH radicals generated from H_2O_2 and Fe(II). The oxidation was stopped by removing the oxidative solution (OH radicals) using centrifugation at 5000 × *g* at 4 °C for 5 min and further quenched with washing with 50 mM ice-cold Tris-HCl (pH 8.0) three times (4, 9). Experiments were done in duplicates.

Footprinting Study of Voltage Gating in Vivo—In this study, cells in midlog growth phase were harvested, centrifuged, and washed as described above. They were stimulated by resuspending in different buffers for 0.5 h before being exposed to OH radicals generated by Fenton reagents. The different buffers were: a low pH buffer (300 mM KCl, 20 mM citric acid, pH 3.0), a low ionic strength buffer (5 mM KCl, pH 7.4), and a low pH and low ionic strength buffer (5 mM KCl, 20 mM citric acid, pH 3.0). All three buffers chosen here are not OH radical scavengers and are suitable for the OH radical-initiated oxidation reaction (9).

Extraction and Delipidation of E. coli Outer Membrane Proteins—The enrichment of outer membrane proteins was carried out as described previously (11, 30) with some modifications. Briefly the cell pellet was resuspended in 10 ml of ice-cold 50 mM Tris-HCl (pH 8.0) supplemented with 100 mM DTT and Complete protease inhibitor mixture tablets. The cells were ruptured by liquid nitrogen cracking, and the unbroken cells were removed by centrifugation at 4 °C at 5000 × *g* for 15 min. The supernatant was collected, lyophilized to dryness, resuspended in 50 ml of ice-cold 0.1 M sodium carbonate (pH 11), and incubated at 4 °C for 1 h with gentle stirring. The sodium carbonate-treated membranes were then pelleted down by ultracentrifugation at 125,000 × *g* at 4 °C for 1 h in an Optima™ L-100 XP ultracentrifuge (Beckman Coulter, Inc., Fullerton, CA). The membrane pellet was washed twice with Milli-Q water using centrifugation at 125,000 × *g* at 4 °C for 30 min.

Delipidation of membrane proteins was achieved via protein precipitation with cold acetone at −20 °C for 2 h. After precipitation, the protein pellets were redissolved in 1% SDS, and protein concentration was determined with a bicinchoninic acid kit (Sigma-Aldrich).

One-dimensional Gel Electrophoresis (SDS-PAGE) and In-gel Digestion—150 μg of proteins from different treatment regimes were dissolved in 60 μl of NuPAGE 1 × LDS sample buffer (Invitrogen) supplemented with 100 mM DTT and denatured by boiling at 95 °C for 5 min. 1D gel electrophoresis was carried out using 12% SDS-PAGE. The gel was stained by a Coomassie Blue staining method.

For the identification of the outer membrane proteome of *E. coli*, a whole lane of the control group was cut off into 10 bands according to the molecular weight of the protein located, followed by reduction with 10 mM DTT in 25 mM ammonium bicarbonate at 56 °C for 1 h, alkylation with 55 mM iodoacetamide in 25 mM ammonium bicarbonate solution at room temperature in the dark for 45 min, and digestion by sequencing grade modified trypsin (Promega Corporation, Madison, WI) digestion in a 1:100 (trypsin:protein) mass ratio at 37 °C overnight.

For the specific study of porin OmpF, the 37-kDa (OmpF) gel bands from each group were excised followed by DTT reduction, iodoacetamide alkylation, and tryptic digestion as described above. Trypsin-digested peptides were then analyzed by LC-MS/MS.

LC-MS/MS Analysis—The LC-MS/MS analysis was done in an LTQ Orbitrap (Thermo Fisher Scientific Inc., Bremen, Germany) as described previously with some modifications (4, 31). The tryptic peptides were reconstituted to 100 μl of 0.1% formic acid (FA) in HPLC water. The samples were then injected by an autosampler and on-line desalted in a Zorbax peptide trap (Agilent, Pola Alto, CA). The peptides were separated by HPLC (Shimadzu, Kyoto, Japan) using a home-packed nanobored C18 column (75-μm inner diameter × 10 cm, 5-μm particles) directly into a picofrit nanospray tip (New Objective, Woburn, MA) operating at a flow rate of about 200 nl/min after a splitter. Buffer A (99.9% H_2O, 0.1% FA) and buffer B (99.9% ACN, 0.1% FA) were used for the LC gradient. The 90-min gradient was ramped from 5% ACN to 30% ACN in 65 min, then to 60% ACN in 10 min, and to 80% ACN over 2 min and then was kept at 80% ACN for 3 min and ramped back to 5% ACN for the last 10 min. The LTQ was operated in a data-dependent mode by performing MS/MS scans for the maximum 10 most intense peaks (ion selection threshold of 500 counts) from each Orbitrap MS scan. Samples were injected into the MS with an electrospray potential of 1.8 kV without sheath or auxiliary gas flow. Ion transfer tube temperature was 180 °C, and collision gas pressure was 0.85 millitorr. The MS scan range was 350–2000 *m/z*. Peptide charge state screening was activated in the Orbitrap MS scan. Dynamic exclusion was activated for the MS/MS scan with a repeat count of 1 and exclusion duration of 20 s. Isolation width was 2 Da, and default charge state was 5. For collision-activated disso-

TABLE I

OMPs with their Mowse scores ranked in the top 10

The sequence coverage of each protein was calculated according to the ratio of the amino acid sequence identified by MS analysis and the whole sequence of the protein.

Index	Protein	Mowse score	Total amino acid sequence	Sequence identified by MS	Sequence coverage
					%
1	P02931; OMPF_ECOLI	64,235	362	334	92.27
2	P0A910; OMPA_ECOLI	24,378	346	309	89.31
3	P69776; LPP_ECOLI	18,111	78	75	96.15
4	P0A940; YAET_ECOLI	9,080	810	637	78.64
5	P02930; TOLC_ECOLI	4,824	493	375	76.06
6	P31554; OSTA_ECOLI	4,430	784	500	63.78
7	P02943; LAMB_ECOLI	2,595	446	325	72.86
8	P0A927; TSX_ECOLI	1,705	294	212	72.11
9	P77774; YFGL_ECOLI	1,691	392	322	82.14
10	P10384; FADL_ECOLI	1,042	446	295	66.14

ciation fragmentation, normalized collision energy was set to 35%, activation Q was set to 0.25, and activation time was 30 ms. Spectra were acquired in centroid format in raw data files with XCalibur (version 2.0 SR2).

Bioinformatics Analysis, Peak Assignment, and Quantitation of Oxidation—MS/MS data for *E. coli* outer membrane proteome were analyzed by MASCOT (version 2.2.04, Matrix Science, London, UK) against the National Center for Biotechnology Information (NCBI) *E. coli* database (version 4, including 54,969 entries). Carbamidomethylated cysteine was set as a fixed modification, and oxidation at methionine residues was set as a variable modification. Peptide tolerance was 8 ppm. Full enzymatic cleavage by trypsin was selected with a maximum of two missed cleavages allowed.

MS/MS data for footprinting experiments were submitted to the SEQUEST protein sequence database search engine for peptide/protein identification against an in-house *E. coli* database. For SEQUEST protein identification, the raw data were batch-searched with Bioworks Browser (version 3.3, Thermo Fisher Scientific Inc.). A maximum of eight post-translational modifications were allowed for a single peptide. Peptide tolerance was 8 ppm, and fragment ion tolerance was 1 amu.

Full enzymatic cleavage by trypsin was selected with a maximum of two missed cleavages allowed. A mass increase of a +16-Da group for all the amino acid residues and +14 Da for the eight residues Val, Ile, Leu, Lys, Arg, Pro, Glu, and Gln were included as variable modifications. For OmpF where the aromatic amino acids and acidic amino acids play important roles in both its structural and functional features, we took two more variable modification types into account. One caused a mass increase of +32 Da by adding two oxygen atoms to the side chain of the five residues Cys, Phe, Met, Trp, and Tyr, and the other was specific to the side chain of the two residues Asp and Glu resulting in a mass shift of −30 Da. Because OmpF has no cysteine residue in its sequence, we did not take carbamidomethylated cysteine into account.

Matched peptides were filtered by requiring a peptide probability cutoff of 0.05 and XCorr cutoffs of 1.0, 2.0, and 2.5 for +1, +2, and +3 charged peptides, respectively. Quantitation of peptide was based on the integrated area of the extracted ion chromatogram (XIC) of precursor ions with mass tolerance of 0.05 Da by Bioworks Browser software. The XICs of precursor ions were confirmed by manual extraction from the MS raw data with a mass tolerance of 5 ppm of the calculated *m/z* values.

A label-free approach was used here to quantify the oxidation levels of the oxidized peptide products of each tryptic peptide arising from the Fenton reaction with OH radicals. As shown in the equation below, by integrating the XIC chromatographic peak areas of both the non-oxidized peptide ions (A_0) and its oxidized counterparts (A_i, $i = 1, 2, \ldots$), we could obtain the relative abundance of each species and quantify the oxidation level.

$$\mathrm{Oxi}_{(i)}\,\% = \frac{A_i}{A_0 + \sum_i A_i} \times 100\% \qquad \text{(Eq. 1)}$$

The data were also analyzed by ByOnic (32), which includes an option for OH radical surface mapping (6). This option simultaneously turns on all 12 possible modifications observed in OH radical mapping (9) as listed in the Introduction. Like SEQUEST, ByOnic sets a limit on the number of modifications per peptide, but the limit depends upon the residue content. Any reactive residue (Cys, Met, Trp, Phe, Tyr, and His) can be modified, but at most two non-reactive residues per peptide may be modified. In ByOnic, we also enabled the following non-oxidative modifications: pyro-Glu on N-terminal Glu and Gln, deamidated Asn and Gln, and (on some of the samples) sodiation on any one residue. Precursor mass tolerance was 8 ppm, and fragment tolerance, after recalibration using a quadratic regression curve computed from initial confident identifications, was 0.5 Da.

Calculation of Solvent-accessible Areas of Amino Acids—To determine whether oxidized residues were solvent-accessible, the exact accessible surface area of the molecular surface for macromolecules was calculated by the program Surface Racer 4.0 (33) based on the x-ray crystal structural data of OmpF (Protein Data Bank code 1OPF).

RESULTS AND DISCUSSION

Outer Membrane Proteome of E. coli—A 1D SDS-PAGE method was utilized to separate the OMPs of *E. coli*. The main advantages of MS-based protein structure determination are the superb sensitivity and high throughput. Using 150 μg of enriched *E. coli* outer membrane proteins in the control group, we identified over 600 proteins. Of these, about 100 proteins were annotated as OMPs. The top 10 ranking OMPs based upon Mowse scores are listed in Table I. Some proteins of typical β-barrel structure have been well documented previously. OmpF is a general β-barrel porin for transportation of polar solutes, whereas LamB, also named maltoporin, is a specific porin that facilitates diffusion of maltodextrins and other maltooligosaccharides. OmpA plays a fundamental role

TABLE II
Tryptic peptides of OmpF

The peptides labeled in bold were the short peptides that could not be detected by LC-MS/MS. Nineteen peptides were clearly identified, covering 92% of the OmpF amino acid sequence.

Sequence	Peptide
23–28	**AEIYNK**
29–38	DGNKVDLYGK
39–47	AVGLHYFSK
48–64	GNGENSYGGNGDMTYAR
65–68	**LGFK**
69–102	GETQINSDLTGYGQWEYNFQGNNSEGADAQTGNK
103–104	**TR**
105–111	LAFAGLK
112–122	YADVGSFDYGR
123–154	NYGVVYDALGYTDMLPEFGGDTAYSDDFFVGR
155–162	VGGVATYR
163–182	NSNFFGLVDGLNFAVQYLGK
183–185	**NER**
186–189	**DTAR**
190–218	RSNGDGVGGSISYEYEGFGIVGAYGAADR
219–231	TNLQEAQPLGNGK
232–241	KAEQWATGLK
242–257	YDANNIYLAANYGETR
258–265	NATPITNK
266–275	FTNTSGFANK
276–299	TQDVLLVAQYQFDFGLRPSIAYTK
300–303	**SKAK**
304–327	DVEGIGDVDLVNYFEVGATYYFNK
328–345	NMSTYVDYIINQIDSDNK
346–362	LGVGSDDTVAVGIVYQF

for the integrity of the bacterial cell surface. It is composed of an N-terminal membrane-embedded domain of 170 residues, serving as a membrane anchor, with an eight-stranded β-barrel structure and a C-terminal 155-residue domain, which is located in the periplasmic space and has been proposed to interact specifically with the peptidoglycan layer (14, 34). TolC is also of this typical structure, and it functions as an energy-dependent transporter (14, 35).

Although we used a much lower amount of starting material (150 μg of membrane proteome) as compared with x-ray and NMR methods for which milligrams of pure single protein would be needed, the average sequence coverage of the top 10 OMPs identified was as high as 79%, indicating the possibility of using an MS-based technique to elucidate the protein structure for these proteins. The protein OmpF, a structurally and functionally well characterized protein, was identified with higher than 90% sequence coverage and was thus chosen as our model protein for further structural analysis. A total of 19 peptides, which represents 92% sequence coverage of OmpF were repeatedly identified by LC-MS/MS (Table II). Several tryptic peptides (in bold in Table II) were not detected, which contributed to a more than 6% sequence loss. These peptides were relatively short, most of them consisting of only two to four amino acids, which might be missed by the precursor ion scan from 350 to 2000 Da. In addition, short tryptic peptides are relatively hydrophilic, resulting in the poor retention in the C18 reverse phase peptide trap or column.

Identification/Detection of Oxidized Peptides of OmpF by LC-MS/MS Analysis—The schematic representation of the *in vivo* membrane protein structure probing process is shown in Fig. 1.

Trypsin-digested peptides of OmpF were analyzed quantitatively by LC-MS/MS. For the positive identification of modification sites, two different database search tools, SEQUEST and ByOnic, were used. For SEQUEST database searching, we included four mass modifications +14, +16, +32, and −30 Da as variable modifications. To minimize false positives, only common modifications identified by both programs were counted even though ByOnic considers a suite of 12 possible oxidative modifications, including some quite uncommon ones.

The six most reactive residues, Cys, Met, Trp, Phe, Tyr, and His, oxidize very readily and thus serve as both positive and negative probes: a cysteine or methionine that does not react is probably not exposed. The less reactive residues serve mainly as positive probes because even highly exposed residues may oxidize at too low a rate to gather meaningful statistics (9).

Identification of modification sites was further confirmed by manually checking the mass spectra. Special attention was paid to the *b*-type fragment ions, which retain the original N terminus of the peptides, and *y*-type fragment ions, which retain the original C terminus. A *b*-type ion that retains only the N-terminal residue would be noted as *b1*, and its sister ion with two residues would be *b2* and so on; the same applies to *y*-type ions *y1*, *y2*, and so on from the C terminus. The mass difference between *b2* and *b1* provided information on the identity of the second residue from the N terminus. Thus, the sequence of the fragmented peptide can be inferred to the extent that sufficient fragment ions are observed. Exact placement of a +16-Da modification is sometimes quite difficult with either SEQUEST or ByOnic and even with manual analysis, and some spectra may in fact represent a mixture of two or more isoforms, the same peptide with a single +16-Da modification in several different sites. Exact placements are more reliable if found independently by two different protein sequence database search engines and confirmed by manual inspection.

Oxidized peptide can be detected by the increased or decreased peptide with mass increase of 16 or 14 Da. In addition, it can be confirmed by inspecting the XIC of the peptide precursor ion. Oxidized peptides are more hydrophilic due to the addition of oxygen and are eluted slightly earlier than the unoxidized counterparts when peptides are separated by reverse phase HPLC. By integrating the XIC areas of the unoxidized and the corresponding oxidized peptides, the abundance of oxidized and unoxidized peptides derived from different regions in OmpF is obtained.

By this way, from the 19 tryptic peptides of OmpF identified, six peptides and 19 amino acids from these six peptides

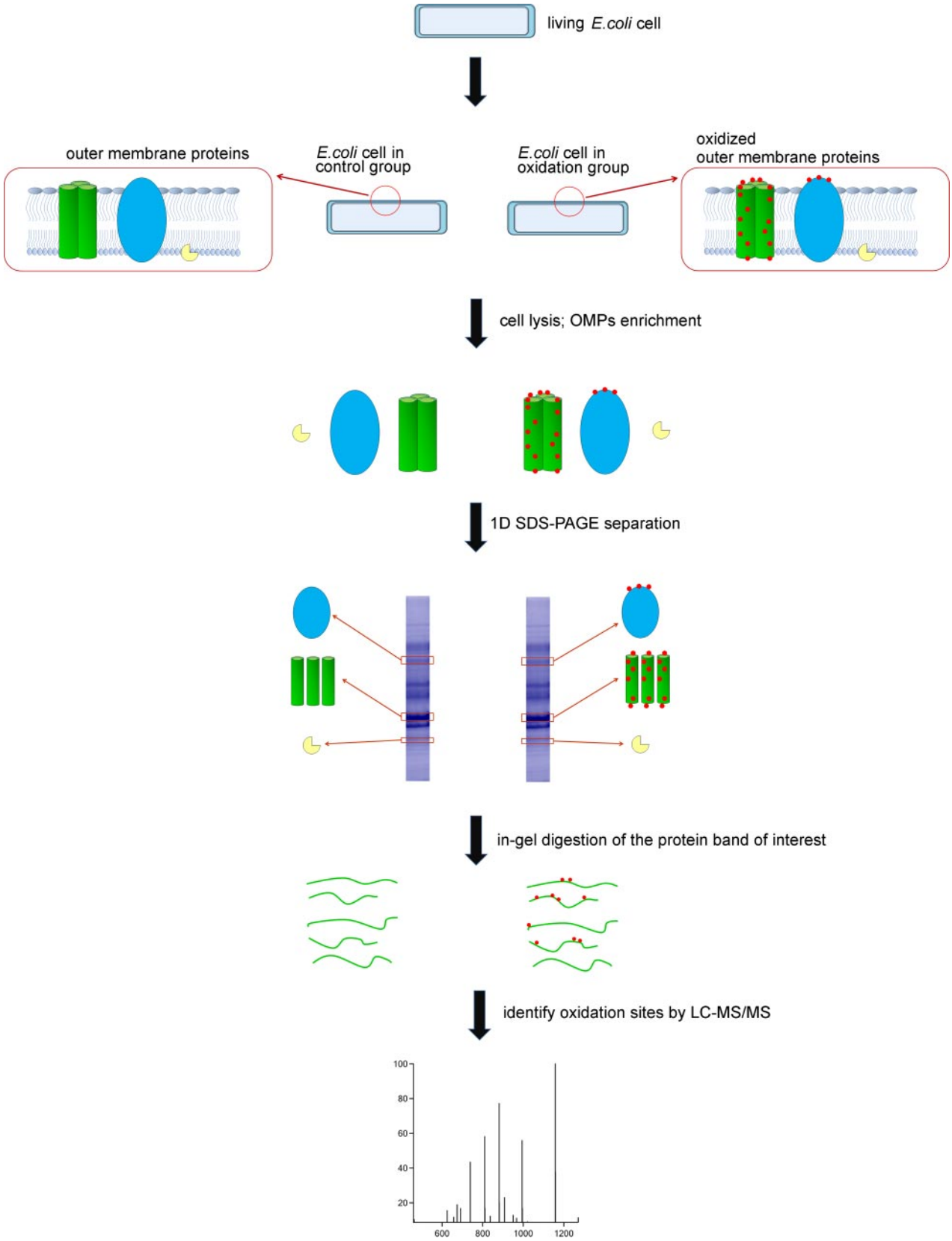

FIG. 1. **The schematic representation of the footprinting process of outer membrane proteins in living *E. coli* cells as described under "Experimental Procedures."**

TABLE III

Oxidation pattern and the corresponding oxidation extent of the six peptides derived from extracted ion chromatogram

The oxidation extent (Oxi) of modified peptides was averaged from duplicate experiments (with the standard deviations seen in Fig. 5). O16, peptide precursor mass increased by 16 Da.

Location	Sequence	Peptide	Oxidation pattern	Oxi	
				Control	Oxidation
				%	
L1	48–64	GNGENSYGGNGDMTYAR	O16	0	100
β4	105–111	LAFAGLK	O16	0	8.1
L3	123–154	NYGVVYDALGYTDMLPEFGGDTAYSDDFFVGR	O16	1	100
β7	163–182	NSNFFGLVDGLNFAVQYLGK	O16	0	6.4
L6	266–275	FTNTSGFANK	O16	0	9.7
β15	328–345	NMSTYVDYIINQIDSDNK	O16	31.8	35.7
			2 O16	0	9.8

TABLE IV

Number of oxidations detected by LC/MS and reactive amino acid residues identified by LC/MS/MS for OmpF

The solvent-accessible surface areas were calculated using Surface Racer 4.0 using the x-ray structure of OmpF. Site locations of the amino acids are listed in column 1. AA, amino acid; SASA, solvent-accessible surface area.

Location	Sequence	Peptide	Oxidized AA	Mass shift	SASA by x-ray
				Da	*Å²*
L1	48–64	GNGENSYGGNGDMTYAR	Asp-59	16	69.91
			Met-60	16	59.28
			Tyr-62	16	27.28
β4	105–111	LAFAGLK	Leu-110	16	93.93
L3	123–154	NYGVVYDALGYTDMLPEFGGDTAYSDDFFVGR	Tyr-133	16	14.77
			Asp-135	16	52.46
			Met-136	16	72.52
			Leu-137	16	16.54
β7	163–182	NSNFFGLVDGLNFAVQYLGK	Asp-171	16	123.86
			Phe-175	16	54.38
			Val-177	16	38.97
			Tyr-179	16	119.55
L6	266–275	FTNTSGFANK	Phe-266	16	138
			Asn-268	16	121.68
			Ser-270	16	47.12
β15	328–345	NMSTYVDYIINQIDSDNK	Met-329	16	58.33
			Tyr-332	16	15.04
			Val-333	16	69.4
			Tyr-335	16	76.6

were reproducibly detected to be oxidized in the oxidation group both by SEQUEST and ByOnic searching methods as shown in Table III and Table IV. Table III lists both the oxidation pattern and the corresponding oxidation extent of each peptide derived from XIC. The extent of oxidation in the modified peptides was averaged from two independent experiments. In Fig. 2, the XICs of oxidized and unoxidized doubly charged peptide ions from tryptic peptide 328–345 "NMSTYVDYIINQIDSQNK" are shown. The chromatographic areas of peptide ions were integrated and used for quantitation of the extent of modification.

As shown in Table III, five peptides with amino acid sequences 48–64, 105–111, 123–154, 163–182, and 266–275, respectively, were oxidized in the sample as compared with control, whereas another peptide with amino acid sequence 328–345 displayed a significant level of oxidation in both the control and oxidation groups. However, the oxidation level of the modified products, especially of the dioxidation products, was significantly higher in the sample as compared with control as shown in Fig. 2, *A* and *B*. The oxidation background in the control group was mainly from the oxidation of the amino acid Met-329 because methionine is inherently highly reactive and easily oxidized without much external oxidative stress (9).

Some modified peptides might be missed by the current data analysis method because the oxidation products are very complicated, and only a subset of possible modifications has been included in the SEQUEST database research. Interestingly in our study, both SEQUEST and ByOnic identified similar modification sites even though their scoring algorithms differ substantially, indicating that identified modification sites are highly reliable.

Consistency of Footprinting and Crystallographic Data for Porin OmpF—Among the oxidized peptides, the ones annotated as L1 and L6 are loops locating on the extracellular side

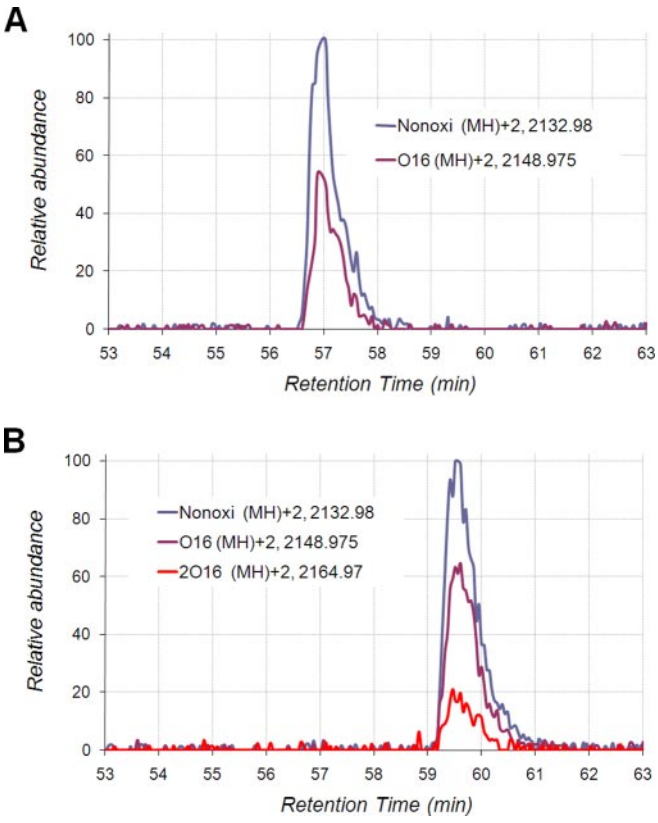

FIG. 2. **The selected ion chromatograms of oxidized and unoxidized doubly charged peptide ions from tryptic peptide 328–345.** *A*, the peptides from the negative control group without oxidation (90-min HPLC gradient). *B*, the peptides from the oxidation group bathed with Fenton reagents in M9 medium (90-min HPLC gradient). *Nonoxi*, non-oxidized; *O16*, peptide precursor mass increased by 16 Da.

of the bacteria that are in contact with the aqueous medium directly. Although L3 folds back into the center of the water channel, it is located right at the entrance of the eyelet, and it remains completely solvent-accessible. Although the polypeptides in the β-stranded area interact with the lipid layer on one side, their other sides are in contact with water inside the channel and are thus susceptible to oxidization by the Fenton reagents. In comparison with the external loops, the oxidation level of the less accessible internal β-barrels should be theoretically lower, and our observation confirmed that the oxidation level of identified β-sheets was indeed far lower than that of the identified external loops as shown in Table III.

Interestingly several loops still remained unoxidized even in the oxidation group, *e.g.* L2 and L4. According to the crystallographic structure of OmpF (20), loops L2 and L4 are important for monomer-monomer interaction in the non-polar core of the porin trimer and will therefore be inaccessible to the solvent and protected from oxidation by the Fenton reagents in the solution. Consistent with this hypothesis, neither L2 nor L4 was found to be oxidized in this study.

The 19 amino acids from the six peptides were widely distributed in the external loop area and internal β-strand area as shown in the reconstituted two-dimensional topology of OmpF in Fig. 3 and 3D structure of OmpF in Fig. 4. We further calculated the solvent-accessible surface area of these amino acids according to their x-ray structure (Protein Data Bank code 1OPF) using Surface Racer 4.0. As displayed in Table IV, consistent with our expectation, all amino acid residues were validated as solvent-accessible.

Footprinting Results Proved the Ion Gating of OmpF Porin Channel in Vivo—It has been reported that the voltage gating of general porins depends on environmental factors like pH, low ionic strength buffer, polycations, polysaccharides, membrane-derived oligosaccharides, and pressure (26, 36–40), implying that the environment-mediated voltage gating of general porins may be a natural protective mechanism of Gram-negative bacteria. Thus we coupled footprinting and environmental factors to probe the surface topology of porin OmpF to determine whether voltage gating occurs *in vivo*. If voltage gating occurs *in vivo*, we expect that there will be some dynamic changes in OmpF in response to changes in ionic environment. Low pH and ionic strength buffer were investigated as two main environmental factors for the *in vivo* study of ion gating.

Fig. 5 shows the extent of oxidation of the five tryptic peptides (the tryptic peptide 266–275 "FTNTSGFANK" located in L6 was lost in some conditions in the experiment, thus we did not take it into account) under different conditions: normal physiological medium (M9 medium), low pH (300 mM KCl, pH 3.0), low ionic strength (5 mM KCl, pH 7.4), or a combination of low pH and low ionic strength (pH 3.0 and 5 mM KCl). Under low ionic strength, low pH, or a combination of both, the oxidation level in loops L1 and L3 remained unchanged from that in the normal physiological condition, whereas that in β-strand areas decreased significantly below that in the normal physiological condition and was just above background level in the control group. As to peptides L1 and L3, only their oxidized counterparts could be easily detected by MS analysis in all four conditions, indicating that they remained highly solvent-accessible. In regard to the amino acid residues of the β-stranded area deep inside the channel, the extent of oxidation significantly decreased. For the tryptic peptide 328–345, the population of its dioxidation products became much smaller and even disappeared. These results demonstrated that few OH radicals could reach this internal β-stranded region to oxidize the amino acids located there.

The significant decrease in the oxidation efficiency of these β-sheet peptides when the cells were exposed to low ionic strength, low pH, or a combination of both is consistent with channel closure of the pore, *i.e.* voltage gating. In this study, the OH radicals used to oxidize the amino acid side chains inside the β-barrel water channels were mainly generated by the reaction of Fe(II) with H_2O_2 *in situ* in the channel. When the channel closed in response to low ionic strength, low pH, or a

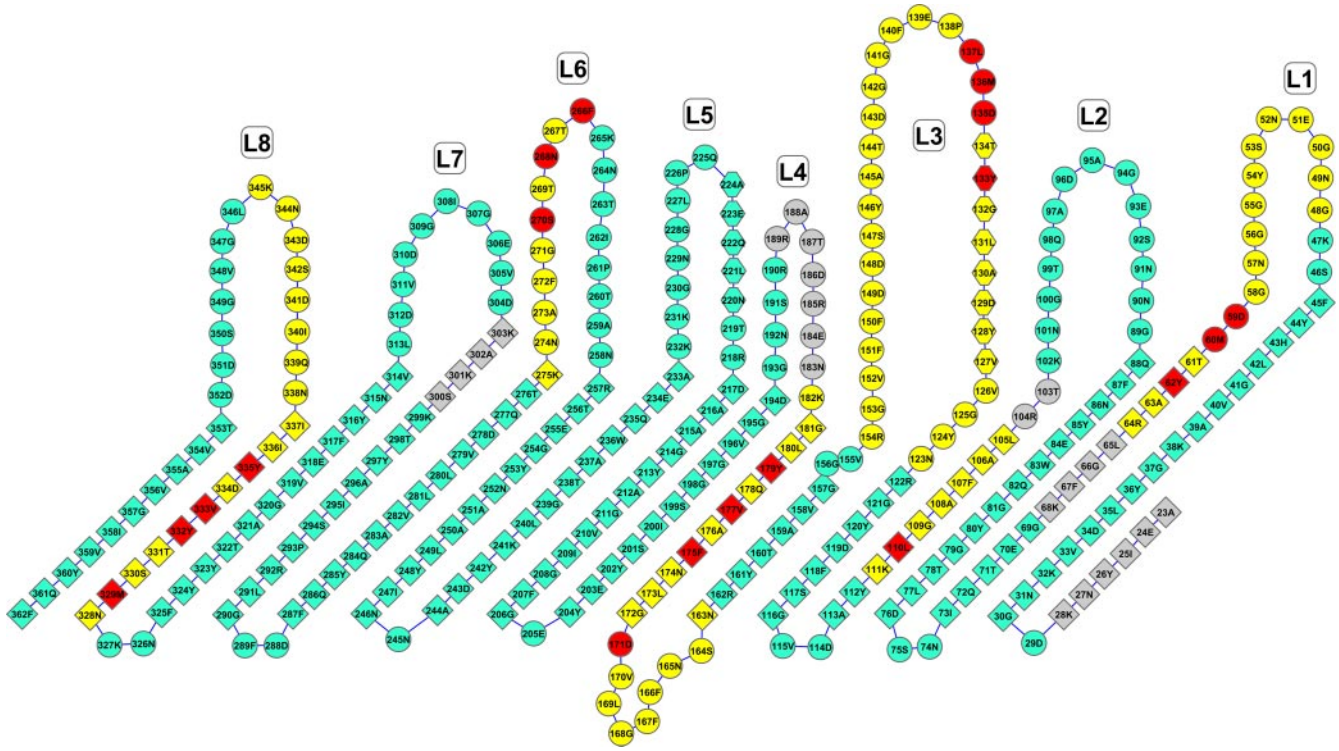

FIG. 3. **Two-dimensional topology of OmpF porin with amino acid sequence in one-letter code.** The view is from outside the 16-stranded antiparallel β-barrel, which is unrolled. Secondary structural elements are indicated by *diamonds* for barrel β-strands, *hexagons* for α-helices, and *circles* for turns and loops. Amino acid sequences labeled in *gray* color were lost and were unable to be detected by MS; the ones labeled in *yellow* were tryptic peptides oxidized in experiments, whereas the ones in *cyan* were non-oxidized. Amino acids labeled in *red* color were recognized by LC-MS/MS analysis as the oxidized sites.

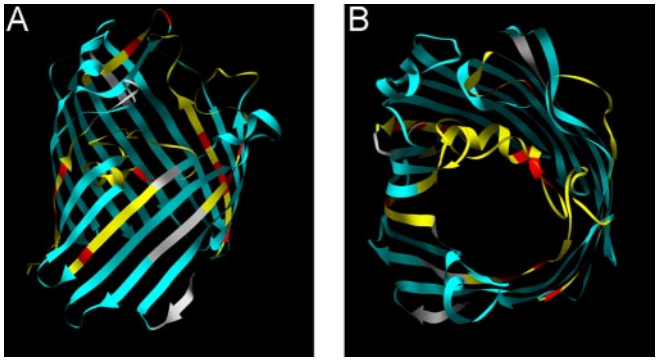

FIG. 4. **3D structures of OmpF monomer from the side view (*A*) and top view (*B*), respectively, according to the footprinting data as well as x-ray data (Protein Data Bank code 1OPF for OmpF).** Peptides detected to be oxidized in experiments are labeled in *yellow* with the specific oxidation sites in *red* color. Non-oxidized peptides are labeled in *cyan*, and peptides unable to be detected are in *gray*.

combination of both, there was a "switch off" of Fe(II) current into the channel, and the Fenton reaction and the subsequent formation of OH radicals were effectively inhibited. Also the high reactivity and short half-life of OH radical make it impossible for any OH radical that is generated outside the channel to passively diffuse into the channel. Therefore when the channel was closed, Fe(II) current would be switched off, the Fenton reaction would not occur, and no OH radical would be generated. Consequently oxidation could not take place.

Footprinting Results Revealed the Molecular Basis of Voltage Gating of OmpF Porin—It has been proposed that large deformation-closing of the solid structure of the porin channel is impossible. In a complete barrel of β-strands, all of the polar main chain atoms are engaged in interstrand hydrogen bonds, and the secondary elements are fixed in a rigid network of hydrogen bonds that cannot be easily broken; structural changes of the barrel thus have been considered theoretically unlikely to happen (20). Therefore porins must have other features relevant to their gating. Several hypotheses for the molecular basis of porin voltage gating have been proposed by researchers (25, 41).

First the eyelet has been considered by some researchers as the likely site of voltage gating with structural change in the barrel considered unlikely. Based on its crystallographic structure, the relatively narrower eyelet passageway within the OmpF porin is formed by folding back of the surface loop L3 into the barrel; thus L3 plays a key role in ion selectivity and transport of larger molecules (20). It is also responsible for voltage gating of porins as has been proved by previous studies (42–45). Two possible mechanisms of voltage gating relevant to loop L3 were proposed: the first is the electrostatic feature of the eyelet region, and the second is the large

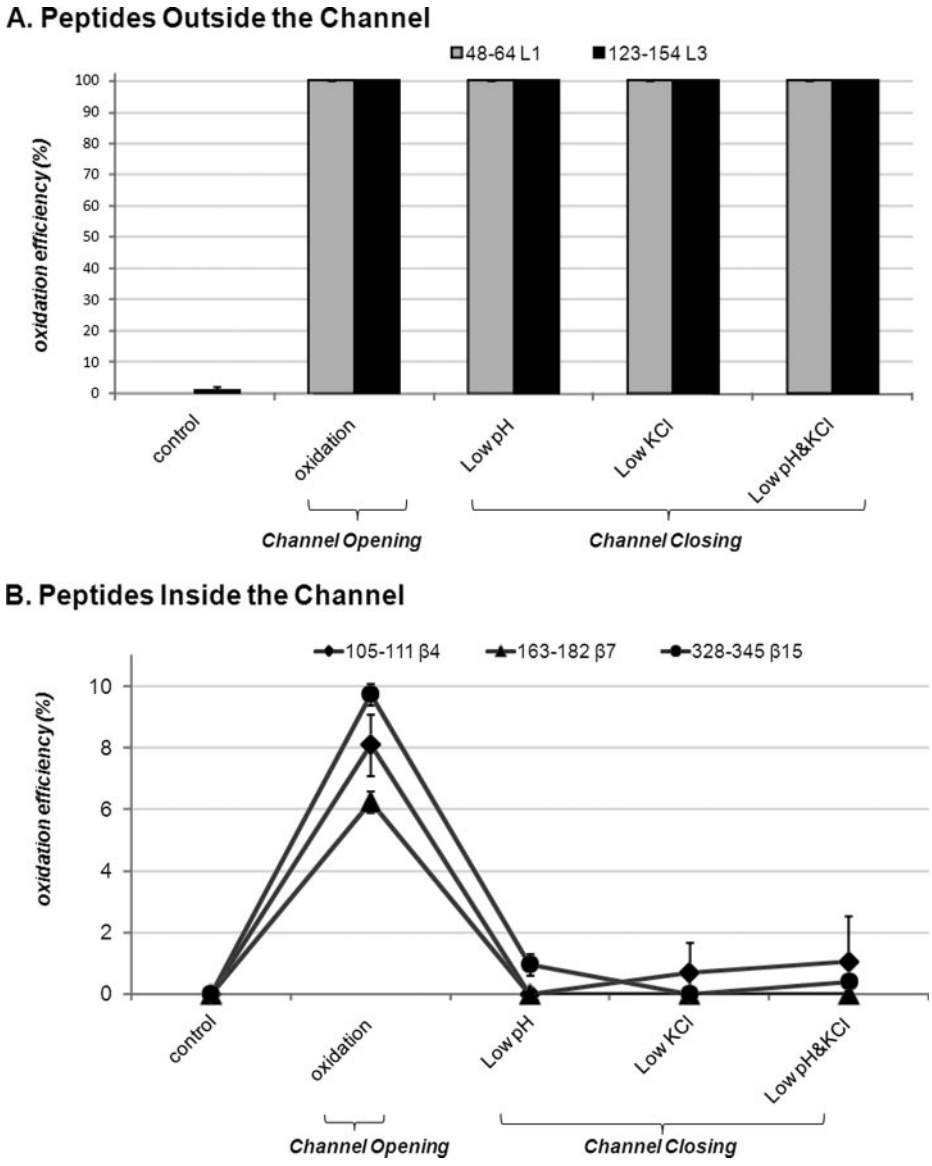

FIG. 5. **Oxidation level of the peptides from different areas, the loop area outside the ion channel and β-stranded area inside the ion channel in different conditions, as shown on the *x axis*.** *A*, the extent of oxidation of loops L1 and L3 kept constant in both channel opening and closing conditions. *B*, the oxidation extent of peptides in β-strand areas fell back to almost the level of control group in channel closing conditions. The *error bars* are standard deviations.

motion of L3 that closes the channel lumen (25, 41). However, the movement of L3 has been proven to be unlikely by previous mutagenesis experiments (42, 46–48). Therefore the former proposed mechanism that the local electrostatic field changes in the eyelet region in response to environmental changes may alter the channel to switch the conductivity of ions has become widely accepted. Another proposed mechanism is the movement of surface loops folding back into porins under certain circumstances. According to the study by Müller and Engel (23) based on atomic force microscopy, the height of OmpF above the lipid matrix is 0.6 nm at low pH or high transmembrane voltage, but the height is 1.3 nm at neutral pH or without transmembrane voltage, and this conformational change is reversible. Based on this observed phenomenon, they further hypothesized that extracellular loops act as the door of the porin channel, and when loops protrude outside the channel, the door is open, and once they fold back inside the channel, the door would be closed, thereby inhibiting the ion current across the channel.

With the deformation of the solid structure of the β-barrel and large motion of loop L3 considered unlikely, our results are opposite to the door closing hypothesis above. According to our footprinting data *in vivo*, the interior L3 polypeptide still remained oxidized even in the "closed state" of the channel, indicating that L3 was surrounded by Fe(II) and H_2O_2 in the pore and that the entrance of the channel had not been blocked by extracellular loops. If the extracellular loops indeed folded back to close the entrance of the channel, L3 should be protected and should have remained as non-oxidized; meanwhile the oxidation efficiency of the superficial loop L1 polypeptide would decrease to some extent rather than remaining the same in this case.

To our current knowledge, acidic residues Asp-135 and Glu-139 of L3 (Asp-113 and Glu-117 according to the x-ray

structure because the N-terminal 1–22 amino acid sequence is lost in the crystallography data) and a cluster of basic residues, Arg-64, Arg-104, and Arg-154 (Arg-42, Arg-82, and Arg-132 in the x-ray structure), on the barrel wall opposite the loop give rise to a transverse electrostatic field, which is essential for ion diffusion (49, 50). The electrostatic field strength has a close relationship with the membrane-bathing solution, especially with its salt concentration (51). Replacing of the minimum salts medium M9 with salt concentration 130 mM with 5 mM KCl in our study weakened the electrostatic field and affected Vc (critical voltage above which the ion channel will be switched off), which caused the channel closure. Meanwhile the charged state of the residues in the eyelet region can also have a significant effect on Vc, and changing the charge state of these residues may change the Vc thus affecting voltage gating according to previous mutagenesis studies (34, 43–46, 52, 53). In our study, when the bacteria were bathed in a pH 3 buffer, the acidic residues (Asp-113 and Glu-117) of L3 would be neutralized by protonation of the carboxylic groups, and the charged states of these two residues would thus be changed. These were of the same effect as the mutations of physiologically negatively charged Asp (Glu) with either neutralized Asn (Gln) or positively charged Lys, and our results were consistent with the mutagenesis studies (44, 45, 52).

Conclusion—In conclusion, we have adapted OH radical surface mapping and its associated MS analysis to probe the surface protein of a living cell. The robustness of this adaptation was verified by the consistency of our surface mapping data of porin OmpF with its current crystallographic structure. In addition, this adaptation also enabled the detection of *in vivo* voltage gating of porin OmpF for the first time. These results suggest that the novel cell surface mapping method coupled with MS analysis is useful to study outer membrane proteins *in vivo*. And we believe that this method is not only suitable for the structural study of OMPs in bacteria, but also it has the potential of being extended to probe the conformational changes of IMPs in mammalian cells.

* This work was supported by Nanyang Technological University, University Research Committee Grant RG61/06 and Ministry of Education of Singapore Academic Research Fund Grant T206B3211.

‖ To whom correspondence should be addressed. Tel.: 65-6514-1006; Fax: 65-6791-3856; E-mail: sksze@ntu.edu.sg.

REFERENCES

1. Punta, M., Forrest, L. R., Bigelow, H., Kernytsky, A., Liu, J., and Rost, B. (2007) Membrane protein prediction methods. *Methods* **41,** 460–474
2. Tullius, T. D., and Dombroski, B. A. (1985) Iron(II) EDTA used to measure the helical twist along any DNA molecule. *Science* **230,** 679–681
3. Pogozelski, W. K., McNeese, T. J., and Tullius, T. D. (1995) What species is responsible for strand scission in the reaction of $[Fe^{II}EDTA]^{2-}$ and H_2O_2 with DNA? *J. Am. Chem. Soc.* **117,** 6428–6433
4. Aye, T. T., Low, T. Y., and Sze, S. K. (2005) Nanosecond laser-induced photochemical oxidation method for protein surface mapping with mass spectrometry. *Anal. Chem.* **77,** 5814–5822
5. Hambly, D. M., and Gross, M. L. (2005) Laser flash photolysis of hydrogen peroxide to oxidize protein solvent-accessible residues on the microsecond timescale. *J. Am. Soc. Mass Spectrom.* **16,** 2057–2063
6. Charvátová, O., Foley, B. L., Bern, M. W., Sharp, J. S., Orlando, R., and Woods, R. J. (2008) Quantifying protein interface footprinting by hydroxyl radical oxidation and molecular dynamics simulation: application to galectin-1. *J. Am. Soc. Mass Spectrom.* **19,** 1692–1705
7. Sharp, J. S., Becker, J. M., and Hettich, R. L. (2003) Protein surface mapping by chemical oxidation: structural analysis by mass spectrometry. *Anal. Biochem.* **313,** 216–225
8. Bohon, J., Jennings, L. D., Phillips, C. M., Licht, S., and Chance, M. R. (2008) Synchrotron protein footprinting supports substrate translocation by ClpA via ATP-induced movements of the D2 loop. *Structure* **16,** 1157–1165
9. Xu, G., and Chance, M. R. (2007) Hydroxyl radical-mediated modification of proteins as probes for structural proteomics. *Chem. Rev.* **107,** 3514–3543
10. Guan, J. Q., and Chance, M. R. (2005) Structural proteomics of macromolecular assemblies using oxidative footprinting and mass spectrometry. *Trends Biochem. Sci* **30,** 583–592
11. Speers, A. E., and Wu, C. C. (2007) Proteomics of integral membrane proteins—theory and application. *Chem. Rev.* **107,** 3687–3714
12. Ruiz, N., Kahne, D., and Silhavy, T. J. (2006) Advances in understanding bacterial outer-membrane biogenesis. *Nat. Rev. Microbiol* **4,** 57–66
13. Schulz, G. E. (1993) Bacterial porins: structure and function. *Curr. Opin. Cell Biol.* **5,** 701–707
14. Galdiero, S., Galdiero, M., and Pedone, C. (2007) beta-Barrel membrane bacterial proteins: structure, function, assembly and interaction with lipids. *Curr. Protein Pept. Sci.* **8,** 63–82
15. Schirmer, T. (1998) General and specific porins from bacterial outer membranes. *J. Struct. Biol.* **121,** 101–109
16. Schulz, G. E. (2000) beta-Barrel membrane proteins. *Curr. Opin. Struct. Biol.* **10,** 443–447
17. Wimley, W. C. (2003) The versatile beta-barrel membrane protein. *Curr. Opin. Struct. Biol.* **13,** 404–411
18. MacKinnon, R. (1995) Pore loops: an emerging theme in ion channel structure. *Neuron* **14,** 889–892
19. Schulz, G. E. (1996) Porins: general to specific, native to engineered passive pores. *Curr. Opin. Struct. Biol.* **6,** 485–490
20. Cowan, S. W., Schirmer, T., Rummel, G., Steiert, M., Ghosh, R., Pauptit, R. A., Jansonius, J. N., and Rosenbusch, J. P. (1992) Crystal structures explain functional properties of two E. coli porins. *Nature* **358,** 727–733
21. Dutzler, R., Schirmer, T., Karplus, M., and Fischer, S. (2002) Translocation mechanism of long sugar chains across the maltoporin membrane channel. *Structure* **10,** 1273–1284
22. Schirmer, T., Keller, T. A., Wang, Y. F., and Rosenbusch, J. P. (1995) Structural basis for sugar translocation through maltoporin channels at 3.1 Å resolution. *Science* **267,** 512–514
23. Müller, D. J., and Engel, A. (1999) Voltage and pH-induced channel closure of porin OmpF visualized by atomic force microscopy. *J. Mol. Biol.* **285,** 1347–1351
24. Samartzidou, H., and Delcour, A. H. (1998) E.coli PhoE porin has an opposite voltage-dependence to the homologous OmpF. *EMBO J.* **17,** 93–100
25. Bainbridge, G., Gokce, I., and Lakey, J. H. (1998) Voltage gating is a fundamental feature of porin and toxin beta-barrel membrane channels. *FEBS Lett.* **431,** 305–308
26. Brunen, M., and Engelhardt, H. (1993) Asymmetry of orientation and voltage gating of the Acidovorax delafieldii porin Omp34 in lipid bilayers. *Eur. J. Biochem.* **212,** 129–135
27. Lakey, J. H., and Pattus, F. (1989) The voltage-dependent activity of Escherichia coli porins in different planar bilayer reconstitutions. *Eur. J. Biochem.* **186,** 303–308
28. Tullius, T. D., and Dombroski, B. A. (1986) Hydroxyl radical "footprinting": high-resolution information about DNA-protein contacts and application to lambda repressor and Cro protein. *Proc. Natl. Acad. Sci. U.S.A.* **83,** 5469–5473
29. Shcherbakova, I., Mitra, S., Beer, R. H., and Brenowitz, M. (2006) Fast Fenton footprinting: a laboratory-based method for the time-resolved analysis of DNA, RNA and proteins. *Nucleic Acids Res.* **34,** e48
30. Fujiki, Y., Hubbard, A. L., Fowler, S., and Lazarow, P. B. (1982) Isolation of intracellular membranes by means of sodium carbonate treatment: application to endoplasmic reticulum. *J. Cell Biol.* **93,** 97–102

31. Sze, S. K., de Kleijn, D. P., Lai, R. C., Khia Way Tan, E., Zhao, H., Yeo, K. S., Low, T. Y., Lian, Q., Lee, C. N., Mitchell, W., El Oakley, R. M., and Lim, S. K. (2007) Elucidating the secretion proteome of human embryonic stem cell-derived mesenchymal stem cells. *Mol. Cell. Proteomics* **6,** 1680–1689
32. Bern, M., Cai, Y., and Goldberg, D. (2007) Lookup peaks: a hybrid of de novo sequencing and database search for protein identification by tandem mass spectrometry. *Anal. Chem.* **79,** 1393–1400
33. Tsodikov, O. V., Record, M. T., Jr., and Sergeev, Y. V. (2002) Novel computer program for fast exact calculation of accessible and molecular surface areas and average surface curvature. *J. Comput. Chem.* **23,** 600–609
34. Hong, H., Szabo, G., and Tamm, L. K. (2006) Electrostatic couplings in OmpA ion-channel gating suggest a mechanism for pore opening. *Nat. Chem. Biol.* **2,** 627–635
35. Koronakis, V. (2003) TolC—the bacterial exit duct for proteins and drugs. *FEBS Lett.* **555,** 66–71
36. Sen, K., Hellman, J., and Nikaido, H. (1988) Porin channels in intact cells of Escherichia coli are not affected by Donnan potentials across the outer membrane. *J. Biol. Chem.* **263,** 1182–1187
37. delaVega, A. L., and Delcour, A. H. (1995) Cadaverine induces closing of E. coli porins. *EMBO J.* **14,** 6058–6065
38. Schindler, H., and Rosenbusch, J. P. (1981) Matrix protein in planar membranes: clusters of channels in a native environment and their functional reassembly. *Proc. Natl. Acad. Sci. U.S.A.* **78,** 2302–2306
39. Delcour, A. H., Adler, J., Kung, C., and Martinac, B. (1992) Membrane-derived oligosaccharides (MDO's) promote closing of an E. coli porin channel. *FEBS Lett.* **304,** 216–220
40. Le Dain, A. C., Häse, C. C., Tommassen, J., and Martinac, B. (1996) Porins of Escherichia coli: unidirectional gating by pressure. *EMBO J.* **15,** 3524–3528
41. Robertson, K. M., and Tieleman, D. P. (2002) Molecular basis of voltage gating of OmpF porin. *Biochem. Cell Biol.* **80,** 517–523
42. Eppens, E. F., Saint, N., Van Gelder, P., van Boxtel, R., and Tommassen, J. (1997) Role of the constriction loop in the gating of outer membrane porin PhoE of Escherichia coli. *FEBS Lett.* **415,** 317–320
43. Mobasheri, H., and Lea, E. J. (2002) Biophysics of gating phenomena in voltage-dependent OmpC mutant porin channels (R74C and R37C) of Escherichia coli outer membranes. *Eur. Biophys. J.* **31,** 389–399
44. Phale, P. S., Philippsen, A., Widmer, C., Phale, V. P., Rosenbusch, J. P., and Schirmer, T. (2001) Role of charged residues at the OmpF porin channel constriction probed by mutagenesis and simulation. *Biochemistry* **40,** 6319–6325
45. Miedema, H., Vrouenraets, M., Wierenga, J., Eisenberg, B., Schirmer, T., Baslé, A., and Meijberg, W. (2006) Conductance and selectivity fluctuations in D127 mutants of the bacterial porin OmpF. *Eur. Biophys. J.* **36,** 13–22
46. Bainbridge, G., Mobasheri, H., Armstrong, G. A., Lea, E. J., and Lakey, J. H. (1998) Voltage-gating of Escherichia coli porin: a cystine-scanning mutagenesis study of loop 3. *J. Mol. Biol.* **275,** 171–176
47. Phale, P. S., Schirmer, T., Prilipov, A., Lou, K. L., Hardmeyer, A., and Rosenbusch, J. P. (1997) Voltage gating of Escherichia coli porin channels: role of the constriction loop. *Proc. Natl. Acad. Sci. U.S.A.* **94,** 6741–6745
48. Saint, N., Lou, K. L., Widmer, C., Luckey, M., Schirmer, T., and Rosenbusch, J. P. (1996) Structural and functional characterization of OmpF porin mutants selected for larger pore size. II. Functional characterization. *J. Biol. Chem.* **271,** 20676–20680
49. Im, W., and Roux, B. (2002) Ions and counterions in a biological channel: a molecular dynamics simulation of OmpF porin from Escherichia coli in an explicit membrane with 1 M KCl aqueous salt solution. *J. Mol. Biol.* **319,** 1177–1197
50. Schirmer, T., and Phale, P. S. (1999) Brownian dynamics simulation of ion flow through porin channels. *J. Mol. Biol.* **294,** 1159–1167
51. Alcaraz, A., Nestorovich, E. M., Aguilella-Arzo, M., Aguilella, V. M., and Bezrukov, S. M. (2004) Salting out the ionic selectivity of a wide channel: the asymmetry of OmpF. *Biophys. J.* **87,** 943–957
52. Bredin, J., Saint, N., Malléa, M., Dé, E., Molle, G., Pagès, J. M., and Simonet, V. (2002) Alteration of pore properties of Escherichia coli OmpF induced by mutation of key residues in anti-loop 3 region. *Biochem. J.* **363,** 521–528
53. Van Gelder, P., Saint, N., Phale, P., Eppens, E. F., Prilipov, A., van Boxtel, R., Rosenbusch, J. P., and Tommassen, J. (1997) Voltage sensing in the PhoE and OmpF outer membrane porins of Escherichia coli: role of charged residues. *J. Mol. Biol.* **269,** 468–472